Flow-Induced Energy Harvesting: Conceptual Design and Numerical Analyses of a Piezoelectric Bender for Smart Building Applications

Sara Ferri, Konstantinos Gkoumas*, Francesco Petrini and Franco Bontempi
sara_ferri86@yahoo.it, konstantinos.gkoumas@uniroma1.it, francesco.petrini@uniroma1.it, franco.bontempi@uniroma1.it
Department of Structural and Geotechnical Engineering, Sapienza University of Rome, Italy

Abstract: This study focuses on the conceptual design and the numerical analysis of an Energy Harvesting (EH) device, based on piezoelectric materials, for the sustainability of smart buildings. Before that, a comprehensive literature review on the topic takes place. The device consists in an aerodynamic fin attached to a piezoelectric element that makes use of the airflow to harvest energy. The principal utilization of this device is for energy autonomous sensors, with applications in smart buildings. A performance-based parametric analysis is conducted (in ANSYS®) in order to assess the optimal values of some design and operating condition parameters, including length, width, thickness, constitutive material of the bender and velocity and turbulence intensity of the incoming airflow. The response parameters used for evaluating the performances include the bender maximum tip displacement, the bender vibration frequency, and the rms of the voltage generated by the device. Considerations are made on possible applications in other sectors (structures and transportations infrastructures).

Keywords: Energy Harvesting, Piezoelectric Materials, Parametric Analysis, FEM Modeling, Building Automation.

Introduction

Engineers, designers and planners, are nowadays very sensitive to issues related to the sustainability of structures. To this end, one of the primary aims of civil engineering design in particular, is to design and build structures with low environmental impact and with an optimal energy performance. Therefore, in the last few decades, the concept of Smart Building was born. This requires buildings equipped with additional subsystems for managing and controlling energy sources and house appliances, and minimize energy consumption, often using wireless communication technology (Morvaj *et al.* 2011). Among these, typical examples are Building Automation Systems, or centralized, interlinked networks of hardware and software that monitor and control the environment in commercial, industrial, and institutional facilities. One of the objectives of Building Automation is to automatize the systems present in the building through the monitoring of ambient parameters using sensors installed in the structure. These sensors can be powered through the mains or in alternative, can be self-powered. The latter is advantageous because it makes their installation easier and it reduces the cost of cabling. An alternative is the use of batteries, which, however, considering their limited lifetime, need to be replaced at regular intervals, so, in addition to having a high environmental impact, their use affects maintenance costs in the long term. Therefore, the best solution is to employ wireless autonomous sensors powered by Energy Harvesting devices.

On the other hand, energy harvesting, i.e. the process of extracting energy from the environment or from a surrounding system and converting it to useable electrical energy, is a prominent research topic, with many promising applications nowadays in buildings, transportation infrastructures and bridges. Its areas of application are currently focused - though not limited - to powering small autonomous wireless sensors (thus eliminating the need for wires), while more recently proposals have been made concerning higher power energy harvesting devices, in the upward trend of renewable energy growth.

Regarding applications for building automation, the trend is very positive in the last years, especially after issues regarding the wireless network frequency allocation have been resolved.

In this paper, a device for converting mechanical energy into electrical energy has been studied. This device can be used to power sensors for building automation, and in particular, for sensors placed inside HVAC (Heating, Refrigerating and Air Conditioning) systems, present in centralized form in many commercial, industrial and constitutional buildings. The device exploits the airflow inside the HVAC ducts. A conceptual design of a bender with piezoelectric material (a material that changes its shape when subjected to an electric field, or, focusing

on the opposite effect pertinent to this case, generates an electric field when it is deformed), is studied inside an HVAC duct and subjected to Vortex Shedding phenomenon. The latter occurs when a body, immersed in a current flow, produces a wake made of vortices that periodically detach alternatively from the body itself with a certain frequency.

A parametric study of the bender has been conducted in order to find the configurations capable of generating resonant conditions that produce the highest level of power for the range of velocity typical inside HVAC ducts (2-5 m/s). A Finite Element Model has been created with the program ANSYS® 13, which treats piezoelectric materials, in order to find the optimal configuration for power wireless sensors.

Literature Review

Micro-scale energy harvesting aims to the powering of sensors or other small electronic devices, including those based on MEMS (Micro Electro Mechanical Systems) that require small amounts of energy. The research carried out in the last decade on micro-scale energy harvesting is massive. Applications in the last decade in the civil engineering field focus on the Structural Health Monitoring (SHM) of long span bridges and skyscrapers.

Harb (2011) and Gkoumas (2012) provide an overview, while an extensive review of methods, technologies and issues is found in Priya and Inman (2009). Gibson (2010) provides a review of multifunctional materials, some of which can be deployed in energy harvesting applications. Belleville et *al.* (2010) lay a framework for the functioning of energy autonomous systems, and provide estimated power output values for different harvesting principles. Chalasani and Conrad (2008) provide a survey of different energy harvesting sources for self-powered embedded devices. Gilbert and Balouchi (2008) review the characteristics and energy requirements of typical sensor nodes, indicate possible application, provide potential ambient energy sources and compare energy harvesting devices found in literature. Gammaitoni *et al.* (2011) discuss issues for kinetic (vibration) energy harvesting. At present, piezoelectric energy harvesting has gained most of the attention; however, there are other promising forms of mechanical energy conversion (e.g. using magnetostrictive materials). Davino *et al.* (2011) discuss issues related to the latter.

Even though a great progress took place in the last decade, there are still issues to be solved and margins for improvement in the efficiency of micro-scale energy harvesting. Some of the key issues (power storage efficiency, communication standards, integration of devices, cost of ownership) are discussed in Kompis and Aliwell (2008). The same authors provide a list of international centers of expertise in this field.

Regarding research on energy harvesting using a piezoelectric bender, in many cases, the bender is integrated with an added tip mass and subjected to mechanical vibrations induced by external forcing. In some cases, like the one of this study, the external forcing is represented by an airflow acting on the structure.

Ly *et al.* (2011) study a piezoelectric cantilever sensor with a mass at the free end, both by means of finite element modeling and experiments. The model and the experiment indicate that the second mode of resonant frequency provide a voltage and a bandwidth much higher than the first mode. Zhou *et al.* (2012) study a shear mode piezoelectric cantilever with a proof mass at the free end, and have evinced that the output peak voltage is maximum when the frequency is resonant (63.8 Hz), while it decreases after that. The output peak power has the same trend and it reaches the maximum of 9 mW at the resonance frequency. Wang and Wu (2012) conduct research on the optimal design of a piezoelectric coupled beam structure. In particular, they observed the effects of the size and the location of the piezoelectric patch as well as the excitation frequency on the power-harvesting efficiency. They find that the efficiency decreases when the location of the piezoelectric patch changes from the fixed end of the beam to its free end. The peak value of the voltage is 0.62 V with an angular frequency of 30 rad/s and an excitation amplitude of 0.1 N. Diyana *et al.* (2012) investigate both single and comb-shaped piezoelectric beam structures, obtaining better results in terms of output voltage for the comb-shaped structure. Blazevic *et al.* (2010) propose a modal model of the dynamic behavior of a piezoelectric cantilever beam. They compare the measured performance of commercially available energy scavenger with the results obtained from a FEM, establishing that the device with larger piezoelectric material volume, outputs more power and that the output power is proportional to the tip-mass. Li *et al.* (2010) compare the behavior and the outputs of a piezoelectric cantilever beam with a curved L-shaped mass with the conventional block-shaped mass, and test it on a shoe under walking conditions. The curved L-shaped mass lowers the fundamental frequency and improves the power density in comparison with conventional cantilever piezoelectric power harvesters. Wang and Ko (2010) develop a FEM model of a new piezoelectric energy harvester from flow-induced vibration in order to estimate the generated voltage of the piezoelectric laminate subjected to a distributed load. The experimental results show that an open circuit output voltage of 2.2 VPP (Peak-to-Peak Voltage) and an

instantaneous output power of 0.2 mW are generated, when the excitation pressure oscillates with an amplitude of 1.196 kPa and a frequency of about 26 Hz. Zhu *et al*. (2010) present a design study on the geometric parameters of a piezoelectric cantilever beam with a seismic mass attached to the tip. For the beam, a shorter length, larger width, and lower ratio of piezoelectric layer thickness to total beam thickness provide better results in the case of a fixed mass. For the mass, a shortened mass length and a higher mass height provide better results in the case of variation in the mass length and a wider width and small mass height are better in the case of variation in mass width and height. For the case of a fixed total length, a shorter beam length and longer mass length provide better results. Gao *et al.* (2013) study a Piezoelectric Flow Energy Harvester (PFEH) based on a piezoelectric cantilever with a cylindrical extension. Prototypes are tested in both laminar and turbulent air flows, showing how PFEHs generate higher voltage and power in the turbulent flow rather than in the laminar flow. The turbulent excitation was the dominant driving mechanism of the PFEH with additional contribution from Vortex Shedding excitation in the lock-in region. Up to 30 mW and 4.5 VOC (Open Circuit Voltage) are obtained at 5 m/s wind velocity in a fan test. Song *et al.* (2012) investigate the feasibility of a piezoelectric cantilever beam for converting mechanical vibrations of an operating high-speed Korean train to useful electricity. They have increased the sensitivity of the system by designing thinning cantilever beams and increasing the piezoelectric material dimensions. The peak power output for a piezoelectric system composed by a 43 x 33 x 0.25 mm^2 piezoelectric material on 69 x 37 x 0.25 mm^2 stainless steel, with four masses of 4.75 g each, is 7.76 mW. Ovejas and Cuadras (2011) study a multimodal piezoelectric wind energy harvester. They use commercial films with different areas and thickness. The energy generated is rectified through a diode bridge and delivered to a storage capacitor. They investigate two different wind flows (laminar and turbulent flows) and also two wind incidences (parallel and normal), obtaining better results in terms of power generation by increasing the thickness and by keeping the area in the effective area range characterized by turbulence. The piezoelectric coupling under wind flow in presence of turbulence is better. The power generation is in the order of 0.2 mW.

In literature, two studies present similarities to the performed analyses in this study. Wu *et al.* (2013) develope a cantilever attached to piezoelectric patches and a proof mass, for wind energy harvesting from a cross wind-induced vibration. They study the influence of the length and location of the piezoelectric patches as well as of the proof mass, on the generated electric power, concluding that the optimal location of the piezoelectric patches is close to the middle lower part of the cantilever harvester when the vortex shedding frequency is close to the second resonant frequency of the harvester. The optimal length of the piezoelectric patches depends on their location and the resonant frequency of the harvester can be adjusted by changing the proof mass attached on the top of the cantilever. Weinstein *et al.* (2012) conduct an experimental study of a cantilevered piezoelectric beam excited in a HVAC duct. In their case, the excitation is amplified by the interactions between an aerodynamic fin attached at the end of the piezoelectric cantilever and the vortex shedding downstream from a bluff body placed in the air flow ahead of the fin-cantilever assembly. They find that the addition of this fin to the tip of the piezoelectric bender improves significantly the power generation of a vortex shedding induced energy harvester. Power generation between 100 and 300 μW for flow speeds in the range of 2-5 m/s are sufficient for powering a sensor node of HVAC monitoring systems or other sensors for smart building technologies.

Modelling Approach and Issues

As stated before, this study focuses on a bender in piezoelectric material under Vortex Shedding flow excitation placed inside an HVAC duct. The purpose is to design a bender in a specific material with a piezoelectric patch, which can enter in resonance with the external force deriving from the Vortex Shedding phenomenon. This is because the resonance conditions produce the highest level of power. From a design point of view, this approach is in contrast with traditional civil and mechanical engineering design, since normally the aim is to avoid the resonance conditions.

Vortex Shedding Excitation

The Vortex Shedding phenomenon occurs when a body, immersed in a current flow, produces a wake made of vortices that periodically detach alternatively from the body itself with a certain frequency n_s. This body enters in resonant conditions when the frequency n_s is equal to the natural frequency of the system.

The detachment of alternating vortices causes a transversal force to the flow direction. This force can be expressed by the harmonic law:

$$f_{sL}(t) = F_{L,i}(s) \cdot \sin(2\pi \cdot n_s t)$$

where $F_{L,i}(s)$ is the equivalent static action:

$$F_{L.i}(s) = m(s) \cdot \left(2 \cdot \pi \cdot n_{i,L}\right) \cdot \phi_{i,L}(s) \cdot y_{pL,i} \cdot C_{TR,i}$$

where:

s is the structural coordinate; $m(s)$ is the element mass per unit length; $\phi_{i,L}(s)$ is the modal shape of the i-eigenmode in the transversal direction,

normalized to 1 in the $\bar{s}$ coordinate of maximum displacement , $\phi_{i,L}(\bar{s}) = 1$; $y_{pL,i}$ is the peak value of the transversal displacement of the element, evaluated at the $\bar{s}$ coordinate; $C_{TR,i}$ is an adimensional parameter related to the possibility that critical values of the average wind velocity occur for elevated values of the return period T_R; n_s is the Vortex Shedding frequency which comes from the Strouhal law:

$$n_s = \frac{St \cdot v_m}{b}$$

where St is an adimensional parameter, called Strouhal parameter, which is function of the section shape and the Reynolds number, v_m is the a average flow velocity, and b is the characteristic dimension of the cross-section.

The most critical conditions occur when the frequency n_s is equal to the natural frequency of transversal vibration of the body $n_{i,L}$, in particular when it is equal to the first frequency associated to the eigenmode of vibration perpendicular to the wind direction. When $n_s = n_{i,L}$, the average velocities of the wind are the critical ones and the structure enters in resonant conditions. These conditions produce the highest level of power. Thus, the Vortex Shedding critical velocity for the i-transversal eigenmode, is defined as the average wind velocity that produces resonant conditions, $n_s = n_{i,L}$. The critical velocity can be expressed as:

$$v_{cr} = \frac{n_{i,L} \cdot b}{St}$$

The difficulties arise from the fact that the sinusoidal force generated form the Vortex Shedding, and, therefore, the frequency n_s, depend from the dimensions of the body on which the flow impacts, as well as from the average velocity of the air flow in the HVAC duct. The value of this velocity lies in the range of 2-5 m/s. Therefore, to ensure that the bender enters in resonant conditions, flow velocity must be the critical one for the bender. Following that, if the bender configuration is changed, its eigenmodes of vibration will change, as well as its natural frequency, and hence, its critical velocity. Vice versa, if the flow velocity is changed, the optimal configuration that induces the resonance will change.

Numerical Modeling

The configuration of the piezoelectric bender is shown in figure 1. The object of the research is a cantilever bender with a piezoelectric patch, placed inside an HVAC duct (figure 1a).

The incoming wind flow impacts the bender and the detachment of alternating vortices produces a sinusoidal force acting in transversal direction to the wind flow (figure 1c). This force causes the vibration of the bender (figure 1b). Initially, a simple bender with piezoelectric patches has been studied, and, after the initial results, its configuration was changed, by adding a tip-mass (figure 1b). The geometric parameters of the bender, the patch and the tip-mass are shown in figure 2 and in table 1.

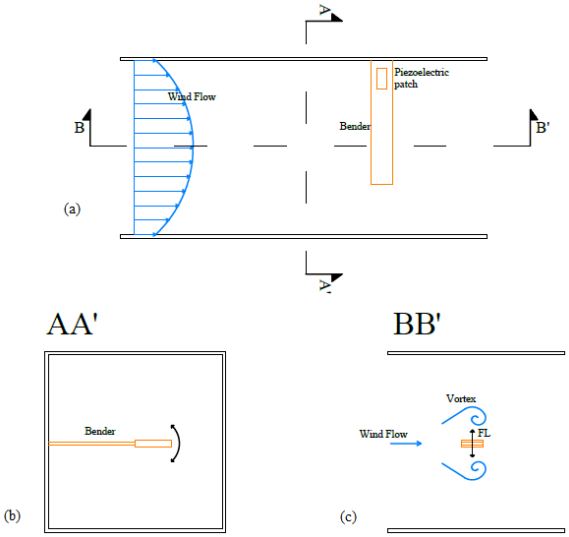

Figure 1. Piezoelectric Bender Inside the HVAC Duct

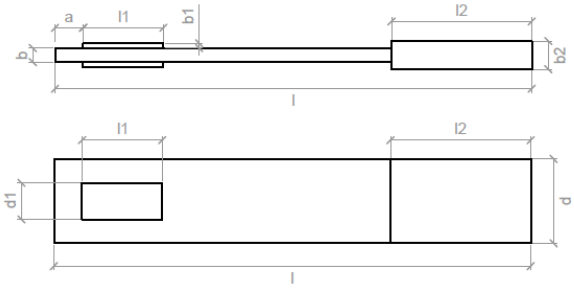

Figure 2. Geometric Parameters

Table 1. Values of Geometric Parameters

ELEMENTS	DIMENSIONS	VALUES (m)
BENDER	l	variable
	b	variable
	d	variable
	a	0.01
PIEZO - ELECTRIC PATCH	l_1	0.0286
	b_1	0.0017
	d_1	0.0127
ADDED MASS	l_2	variable
	b_2	0.01
	d_2	d

As shown in table 1, some dimensions are fixed while other can vary. The (fixed) dimensions of the piezoelectric patch have been chosen according to the piezoelectric elements currently available in the market. For the added mass, a fixed thickness of 0.01 m was chosen. The width of the added mass is the same as the one of the bender, while the length has been modified in order to study how it affects the entire model, as well as the bender dimensions.

In addition, and regarding the materials, the material properties of the piezoelectric patch are fixed while those of the bender can vary. In total, three materials have been considered, in order to identify the one with the optimal characteristics of weight and stiffness for the specific case. The materials and their characteristics are reported in table 2.

Table 2. Material Properties

MATERIAL	E (N/m^2)	ρ (kg/m^3)
Balsa	$3.3 \cdot 10^{12}$	175
Aluminum	$6.4 \cdot 10^{10}$	2700
Lead	$4 \cdot 10^{10}$	7400
LEAD ZIRCONATE TITANATE		
Density ρ	7800 kg/m^3	
Young Modulus E	6.6 $x10^3$ N/m^2	
Poisson ratio υ	0.2	
Relative dielectric constant k^T_3	1800	
Permittivity ε	1.602 $x10^{-8}$ F/m	
Piezoelectric constant d_{31}	-190 $x10^{-12}$ m/V (C/N)	

Numerical Results

In the first instance, and in order to find the most suitable density and stiffness characteristics, the Vortex Shedding parameters and bender modal characteristics have been studied for three different materials, which have been chosen for their different properties. After that, and after deciding that the best configuration is the one with the added tip mass, the length of this mass was calculated for multiple bender dimensions. Finally, the voltage and power outputs are reported as a function of the added mass and as a function of the bender dimensions.

Dimensions and Natural Frequencies

Table 3 provides the range of three variable bender dimensions. For each value, modal analysis was conducted and the Vortex Shedding parameters calculated. A bender modeled in aluminum was implemented in this case; the configuration is not the right one, but it was desired to show only to highlight the dependency from the bender dimensions of the parameters.

Table 3. Bender Dimension Range

Dimension	Range
Length *l*	0.06÷0.20 m
Thickness *b*	0.001÷0.008 m
Width *d*	0.02÷0.05 m

In the following figures, the frequency dependence from the bender dimensions is shown. As can be seen, the frequency increases with the bender thickness (figure 3) and it decreases with the length (figure 4) and the width (figure 5) of the bender.

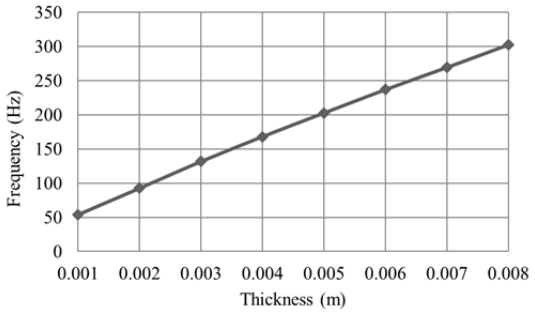

Figure 3. Frequency as a Function of the Thickness

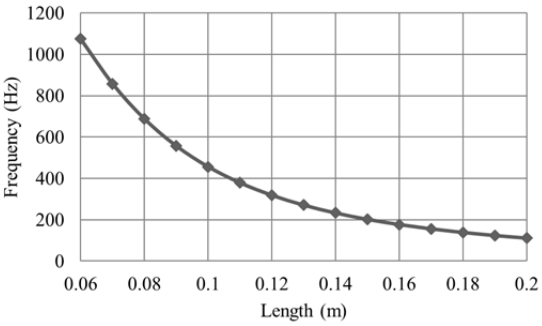

Figure 4. Frequency as a Function of the Length

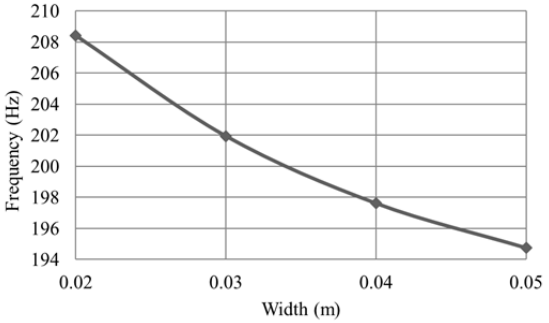

Figure 5. Frequency as a Function of the Width

Critical Velocity and Static Force

Figures 6 to 11 report the results.

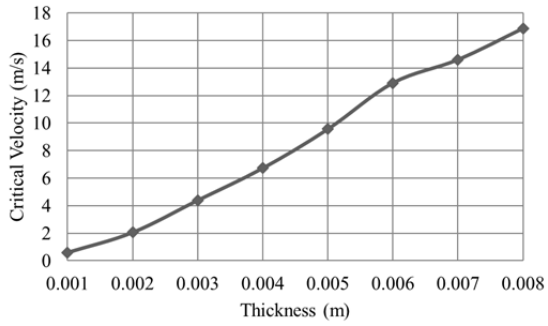

Figure 6. Critical Velocity as a Function of the Thickness

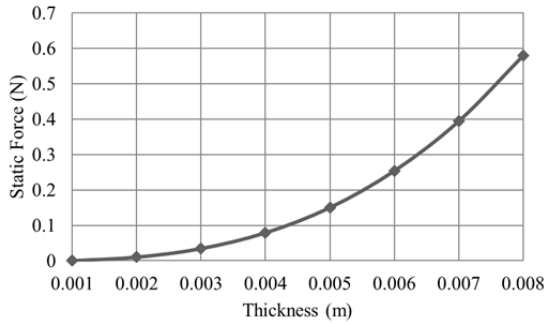

Figure 7. Static Force as a Function of the Thickness

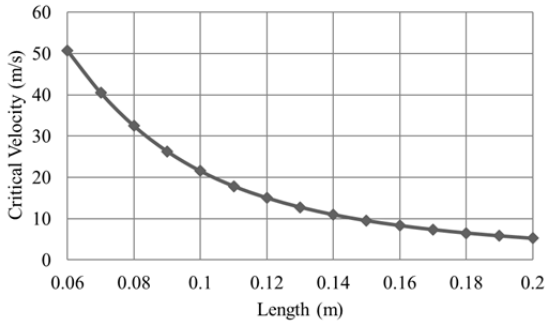

Figure 8. Critical Velocity as a Function of the Length

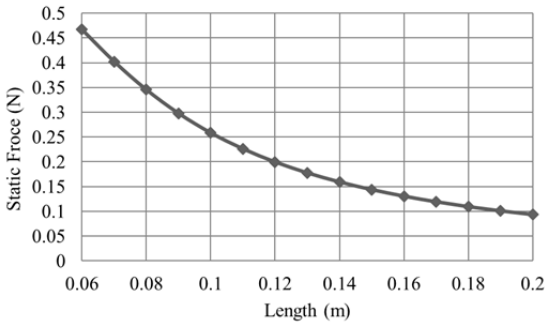

Figure 9. Static Force as a Function of the Length

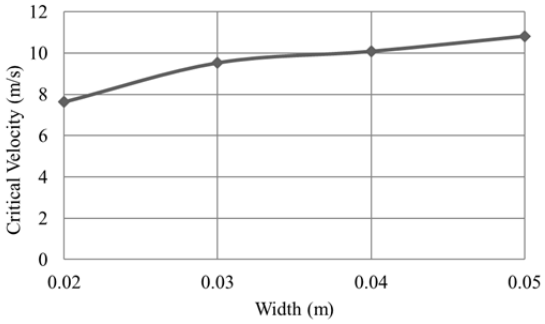

Figure 10. Critical Velocity as a Function of the Width

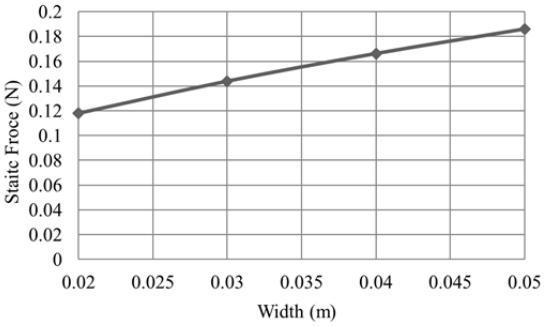

Figure 11. Static Force as a Function of the Width

The critical velocity and the static force are strongly interdependent and, for this reason, they have a similar tendency. They increase according to the thickness and the width, whereas they decrease according to the length of the bender.

Materials

After testing different material, the results of analysis with two materials in particular (aluminum and lead) are reported. The characteristics of the materials are those shown in table 2.

It was decided to show the results with these two materials because of their different densities and stiffness, so it is possible to comprehend the bender behavior to density and stiffness variations. In table 4, the values of the bender dimensions used in this case are reported.

Figures 12 and 14 show the frequency for the model in aluminum and lead respectively, while figures 13 and 15 show the critical velocity for the same materials.

Table 4. Values of Bender Dimensions

Dimension	**Values**
Length *l*	0.15÷0.20 m
Thickness *b*	0.003÷0.006 m
Width *d*	0.03 m

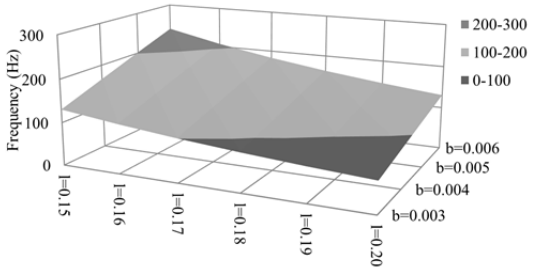

Figure 12. Natural Frequency as a Function of the Length and the Thickness for the Aluminum Model

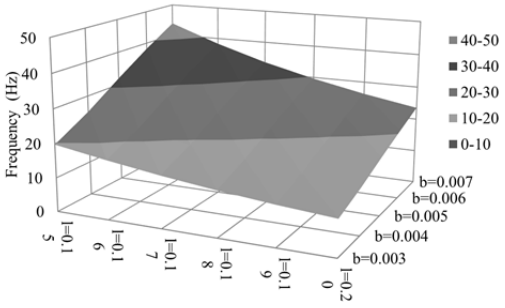

Figure 13. Natural Frequency as a Function of the Length and the Thickness for the Lead Model

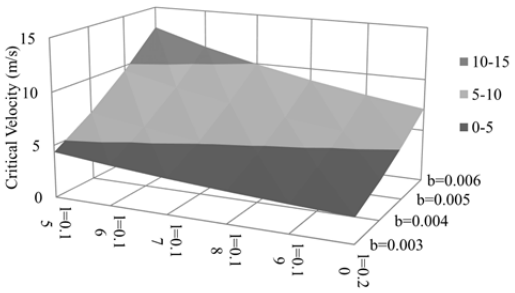

Figure 14. Critical Velocity as a Function of the Length and the Thickness for the lluminium Model

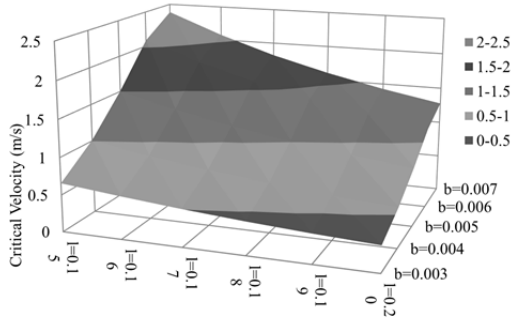

Figure 15. Critical Velocity as a Function of the Length and the Thickness for the Lead Model

In addition to the relationship of the parameters with the bender dimensions, these figures show that the configuration entirely in aluminum is very light. In fact, the critical velocities and the frequencies are too high. On the contrary, the configuration entirely in lead is very heavy and, consequently, the critical velocities are too low. Therefore, an additional configuration is studied in order to obtain the required global density and stiffness: a bender with a tip mass. The addition of the mass allows tuning the natural frequency of the bender and, therefore, the critical velocity.

Addition of a Tip Mass

For the calculation of the tip mass, as well as of its dependency from the dimensions, the following considerations are made.

The critical velocity range is imposed (2-5 m/s), which corresponds to the range of the average velocity in the duct, and from it the Vortex Shedding frequency n_s was calculated. The latter must be equal to the natural frequency n_i of the first eigenmode in order to obtain resonant conditions. Therefore, from the difference between these frequencies (n_s and n_i), the mass size is calculated. Fixing two dimensions, the width and the thickness of the mass, only the mass length was calculated, for each couple *l*-*b* of the bender.

Table 5 shows the values of the bender dimension with which the results are obtained.

Figures 16, 17, and 18 show the required mass length for different values of the critical velocity bender length and the bender thickness respectively.

Table 5. Bender Dimension Range

Dimension	**Values**
Length *l*	0.15÷0.20 m
Thickness *b*	0.003÷0.006 m
Width *d*	0.03 m

The lower the velocity acting in the duct (which is imposed equal to the critical one), the greater the required mass size must be (figure 16). This is because, by increasing the mass, the frequency decreases, and for lower values of the critical velocity lower frequency values are required.

In addition, the results shown in figures 17 and 18 are compatible with what reported before. For example, regarding the length variation, when it increases the natural frequency of the bender without the tip mass decreases. Therefore, the mass to be added in order to lower the natural frequency to the required value decreases. The exact opposite thing happens when considering the thickness variation (figure 18).

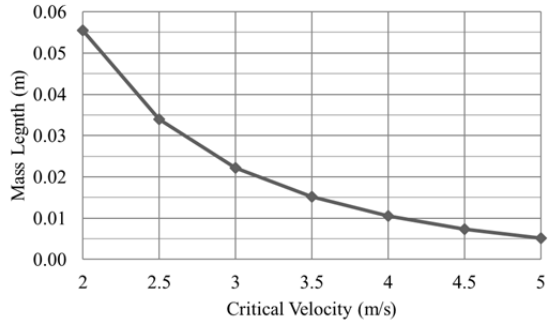

Figure 16. Required Mass Length for Different Critical Velocities

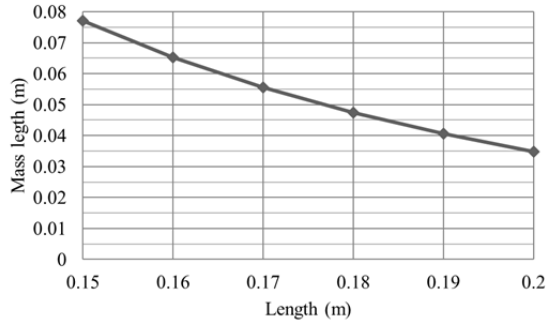

Figure 17. Mass Length as a Function of the Bender Length

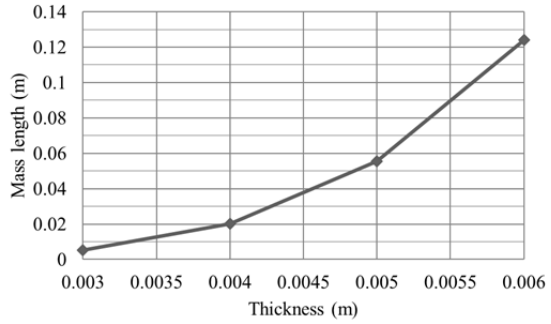

Figure 18. Mass Length as a Function of the Bender Thickness

Voltage and Power Output

The voltage and power outputs obtained by the application of the sinusoidal force derived from Vortex Shedding phenomenon are illustrated. For both parameters, the peak values and the RMS (Root Mean Square) values were calculated. Results for different configuration are reported in order to understand how outputs vary with the considered parameters. For the calculation of the power a resistance of 1000 Ω was used.

Model with Bender in a Material with Intermediate Properties

In order to study how the voltage and power outputs vary with the bender dimensions only (without considering the tip mass), a bender in a material with properties in-between those of aluminum and lead is studied. Table 6 reports the characteristics of this material.

Table 6. Properties of the Fictitious Material

Dimension	Values
Young Modulus E	3.45 x10^{10} N/m^2
Density ρ	7000 kg/m^3

The voltage and power outputs have been calculated both in the center (identified in the figures with "1") and in the corner (identified in the figures with "2") of the piezoelectric patch. The maximum values are measured in the corner, where the stress is maximum. Figures 19, 20 and 21 show RMS and peak values of the voltage for different values of the bender length, the bender thickness and the critical velocity respectively.

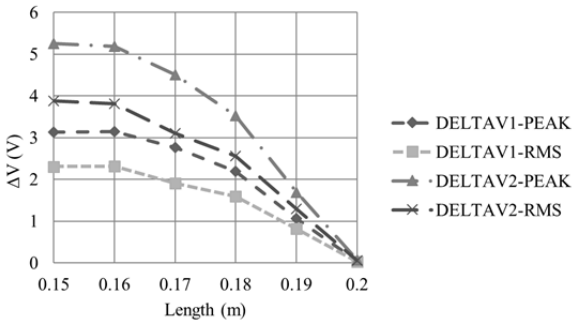

Figure 19. Peak Values and RMS Values of the Voltage for Different Bender Lengths

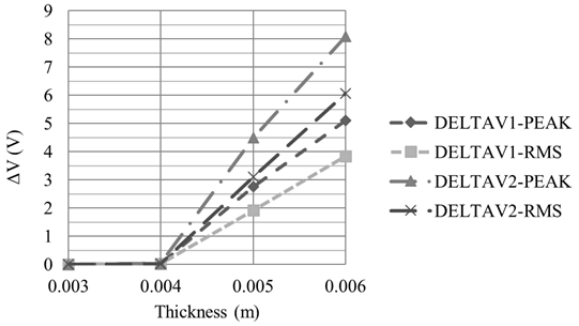

Figure 20. Peak Values and RMS Values of the Voltage for Different Bender Thicknesses

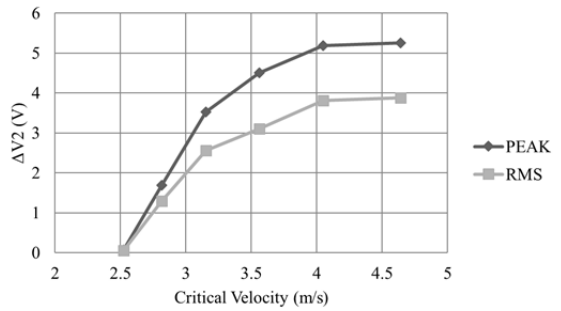

Figure 21. Voltage Output for Different Values of the Critical Velocity

Figures 22, 23 and 24 show the same measures in relation to power.

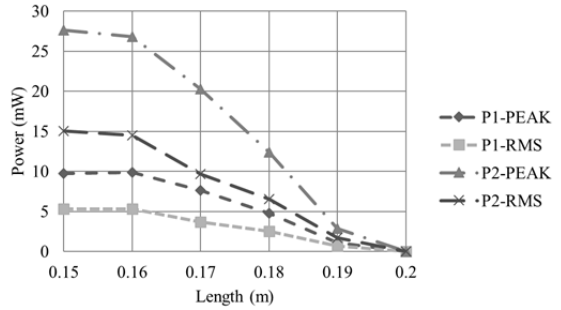

Figure 22. Peak Values and RMS Values of the Power for Different Bender Lengths

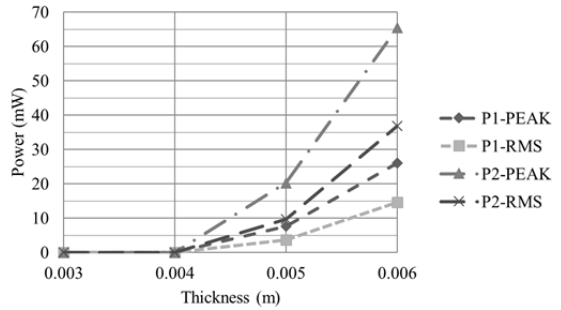

Figure 23. Peak Values and RMS Values of the Power for Different Bender Thicknesses

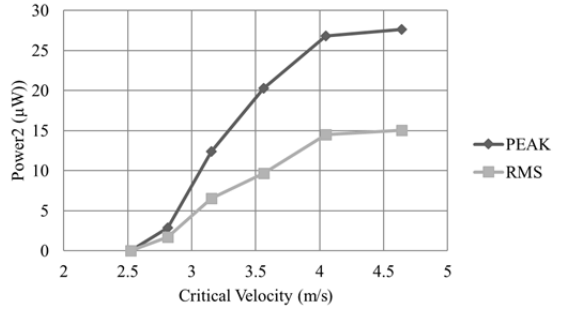

Figure 24. Power Output for Different Values of the Critical Velocity

From the results, it is clear that the voltage output, as well as the power output increase when the thickness increases and the length decreases. The magnitudes of these results are not taken into account, but only the tendencies, because they are obtained through the study of a configuration with a fictitious material. As it is expected, the voltage and the power increase with the critical velocity.

Model with Different Mass Lengths

As a last step, the voltage and power outputs were calculated for a fixed aluminum bender with variable tip mass. The bender dimensions and tip mass dimension are shown in tables 7 and 8 respectively.

Table 7. Bender Dimensions

Dimension	Values
Length l	0.17 m
Thickness b	0.005 m
Width d	0.03 m

Table 8. Added Mass Dimensions

Dimension	Values
Length l_2	variable
Thickness b_2	0.01 m
Width d_2	0.03 m

The peak and RMS values are illustrated in figure 25, for the voltage, and in figure 26, for the output power, which was calculated with a resistance R=1000 Ω. These results show a voltage trend increasing with the added mass, though the trend is not linear but fluctuating. This is caused by the fact that the added mass affects not only the total structure mass, but also the moment of inertia and, therefore, its global stiffness.

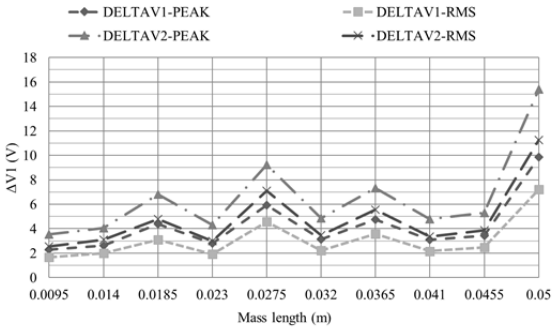

Figure 25. Peak Values and RMS Values of the Voltage for Different Mass Lengths

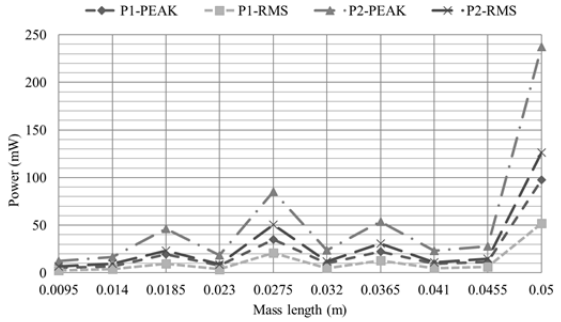

Figure 26. Peak Values and RMS Values of the Output Power for Different Mass Lengths

The maximum voltage output, as well as the maximum power output, occur for the higher mass value (table 9).

Table 9. Maximum RMS and Peak Values of the Voltage and Power Outputs

	VOLTAGE (V)	POWER (mW)
PEAK	15.4	237.20
RMS	11.23	126.25

The above power generation is in line with the energy requirements foreseen in a reference study by Rabaey *et al*. (2000), for the powering of a "PicoNode", a wireless sensing, communication, and computation node that, among else, would consume less than 100 μW on average.

Conclusions

A piezoelectric bender under Vortex Shedding flow excitation placed inside an HVAC duct has been studied. The laws by which the parameters vary have been found, as well as the optimal configuration of the bender and the one that produces the resonance conditions for each value of the airflow velocity acting inside the duct. Finally, the voltage and power outputs have been calculated for different dimensions and configurations. It is found how the critical velocity, the static force and the natural frequency vary with the bender dimensions. The optimal configuration of the bender has also been obtained: a bender made of aluminum with a tip mass made up by lead. The materials were chosen for their stiffness and density characteristics. The added mass allows adjusting not only the total mass of the structure, but also its global stiffness and, as such, it allows tuning the natural frequency of the structure.

The voltage and the power increase when the bender thickness and the critical velocity increase, whereas they decrease when the bender length increases. Furthermore, the voltage and power outputs increase when the added mass increases. The calculated values of the voltage and power are sufficient to power a wireless sensor node in order to monitor ambient parameters inside an HVAC duct.

Of course, there are limitations to this study. In this phase, only the characteristics of the fictitious material have been obtained. For an eventual physical test, a readily available material should be identified. In addition, the results can be considered as preliminary. For an eventual validation, advanced numerical models should be prepared (for example, models based on CFD – Computational Fluid Dynamics), that can better capture the flow-bender interaction. After that, a physical model should be tested in laboratory conditions.

More generally, it is possible to state that energy harvesting technologies make the easy installation of wireless self-powered sensors possible. These can monitor the environmental condition in order to automatize and optimize the operation of specific systems like lighting systems, HVAC (Heating Ventilation and Air Condition) systems, etc. Therefore, the integrated implementation of Building Automation Systems and Energy Harvesting technologies can provide a resolution to the problem of high-energy consumption and elevated cost for maintaining normal function of buildings.

Acknowledgements

This paper presents results from the Master in Science Thesis of one of the authors (Sara Ferri), successfully defended to the Department of Structural and Geotechnical Engineering of the Sapienza Univerity of Rome. The other authors co-advised different parts of this Thesis. Furthermore, the www.francobontempi.org research group at the Sapienza University of Rome is gratefully acknowledged. This study was partially supported by the research spin-off StroNGER s.r.l. (www.stronger2012.com) from the fund "FILAS - POR FESR LAZIO 2007/2013 - Support for the research spin-off".

References

Belleville, M., Fanet, H., Fiorini, P., Nicole, P., Pelgrom, M.J.M., Piguet, C., Hahn, R., Van Hoof, C., Vullers, R. and Tartagni, M. (2010) Energy autonomous sensor systems: Towards a ubiquitous sensor technology. *Micro electronics Journal*, Vol. 41, No. 11, pp. 740-745.

Blazevic, D., Zelenia, S. and Gregov, G. (2010) Mechanical analysis of piezoelectric vibration energy harvesting devices. *MIPRO, 2010 Proceedings of the 33rd International Convention*, pp. 122-126.

Chalasani, S. and Conrad, J.M. (2008) A Survey of Energy Harvesting Sources for Embedded

Systems. *IEEE Proceedings of Southeastcon 2008*, pp. 442–447.

Davino, D., Giustiniani, A. and Visone, C. (2012) Effects of hysteresis and eddy currents in magnetostrictive harvesting devices. *Physica B: Condensed Matter*, Vol. 407, No. 9, pp. 1433-1437.

Dyiana, N. H., Muthalig, A. G. A., Fakhzan, M. N. and Nordin, A. N. (2012) Vibration energy harvesting using single and comb-shaped piezoelectric beam structures: modelling and simulation. *Procedia Engineering*, Vol. 41, pp. 1228-1234.

Gammaitoni, L., Vocca, H., Neri, I., Travasso, F. and Orfei, F. (2011) Vibration Energy Harvesting: Linear and Nonline-ar Oscillator Approaches, Sustainable Energy Harvesting Technologies - Past, Present and Future. Yen Kheng Tan (Ed.), InTech, Retrieved May 27, 2014 from: http://www.intechopen.com/articles/show/title/vibration-energy-harvesting-linear-and-nonlinear-oscillator-approaches

Gao, X., Shih, W-H. and Shih, W. Y. (2013) Flow energy harvesting using piezoelectric cantilevers with cylindrical extension. *IEEE Transactions on Industrial Electronics*, Vol. 60, No. 3, pp. 1116-1118

Gibson, R.F. (2010) A review of recent research on mechanics of multifunctional composite materials and structures. *Composite Structures,* Vol. 92, pp. 2793–2810.

Gilbert, J.M. and Balouchi, F. (2008) Comparison of Energy Harvesting Systems for Wireless Sensor Networks. *International Journal of Automation and Computing*, Vol. 5, No. 4, pp. 334-347.

Gkoumas, K. (2012) Energy harvesting in bridges and transportation infrastructure networks: state of art, recent trends and future developments. *Proceedings of the Sixth International IABMAS Conference*, pp. 1527-1533.

Harb A. (2011) Energy harvesting: State-of-the-art. *Renewable Energy*, Vol. 36, No. 10, pp. 2641-2654.

Kompis, C. and Aliwell, S. (eds.). (2008) Energy Harvesting Technologies to enable remote and wireless Sensing. Sensors and Instrumentation KTN Report, Retrieved May 27, 2014 from: ftp://ftp.cordis.europa.eu/pub/fp7/ict/docs/necs/20090306-05-eharvesting-ck_en.pdf

Li, R., Rguiti, M., D'Atorg, S., Hajjaji, A., Courtois, C. and Leriche, A (2011) Modeling and characterization of piezoelectric cantilever bending sensor for energy harvesting. *Sensors and Actuators A: Physical*, Vol. 168, No. 1, pp. 95-100.

Ly, W. G., He, S. and Yu, S. (2010) Improving power density of a cantilever piezoelectric power harvester through a curved L-shaped proof mass. *IEEE Transaction in industrial electronics*, Vol. 57, No. 3, pp. 868-876.

Morvaj, B, Lugaric, L. and Krajcar, S. (2011) Demonstrating smart buildings and smart grid features in a smart energy city. *Proceedings of the 2011 3rd International Youth Conference on Energetics (IYCE)*, pp.225-232.

Ovejas, V. J. and Cuadra, A. (2011) Multimodal piezoelectric wind energy harvesters. *Smart Materials and Structures,* Vol. 20, 8pp.

Priya, S. and Inman, D.J. (eds). (2009) *Energy Harvesting Technologies*, New York, Springer.

Rabaey, J., Ammer, J., da Silva, J., Patel, D. and Roundy, S. (2000) Picoradio supports ad-hoc ultra-low power wireless networking. *IEEE Computer Magazine*, Vol. 33, No. 7, pp. 42–47.

Song, D., Yang, C. H., Hong, S. K., Kim, S. B., Woo, M. S. and Sung, T. H. (2012) Feasibility study in application of piezoelectricity to convert vibrations of Korea Train Express. *Proceedings of IEEE Applications of Ferroelectrics (ISAF/ECAPD/PFM).*

Wang, D-A. and Ko, H-H. (2010) Piezoelectric energy harvesting from flow-induced vibration. *Journal of Micromechanics and Microengineering*, Vol. 20, No. 2, 9pp.

Wang, Q. and Wu, N (2012) Optimal design of a piezoelectric coupled beam for power harvesting. *Smart Materials and Structures*, Vol. 21, No. 8.

Weinstein, L. A., Cacan, M. R., So, P. M. and Wrigth, P. K. (2012) Vortex shedding induced energy harvesting from piezoelectric materials in heating, ventilation and air conditioning flows. *Smart Materials and Structures.* Vol. 21, 10pp.

Wu, N., Wang, Q. and Xie, X. (2013) Wind energy harvesting with a piezoelectric harvester. *Smart Materials and Structures*, Vol. 22, No. 9.

Zhou, L., Sun, J., Zheng, X. J., Deng, S. F., Zhao, J. H., Peng, S. T., Wang, X. Y. and Cheng, H. B. (2012) A model for the energy harvesting performance of shear mode piezoelectric. *Sensors and Actuators A: Physical,* Vol. 179, pp. 185-192.

Zhu, M., Worthington, E. and Tiwari, A. (2010) Design study of piezoelectric energy harvesting devices for generation of higher electrical power using a coupled piezoelectric-circuit finite element method. *IEEE Transactions on Ultrasonics, Ferroelectrics and Frequency control,* Vol. 57, No. 2, pp. 427-437.